Sādhanā Vol. 42, No. 2, February 2017, pp. 271–280
DOI 10.1007/s12046-017-0592-1

Experimental force modeling for deformation machining stretching mode for aluminum alloys

ARSHPREET SINGH and ANUPAM AGRAWAL*

Department of Mechanical Engineering, Indian Institute of Technology Ropar, Rupnagar 140001, India
e-mail: arshpreet.singh@iitrpr.ac.in; anupam@iitrpr.ac.in

MS received 22 June 2015; revised 20 May 2016; accepted 1 August 2016

Abstract. Deformation machining is a hybrid process that combines two manufacturing processes—thin structure machining and single-point incremental forming. This process enables the creation of complex structures and geometries, which would be rather difficult or sometimes impossible to manufacture. A comprehensive experimental study of forces induced in deformation machining stretching mode has been performed in the present work. A table-type force dynamometer has been used to record the deforming forces in three Cartesian directions. The influence of five process parameters—floor thickness, tool diameter, wall angle, incremental step size, and floor size on the deforming forces—is investigated. Individual as well as combined empirical models of the parameters with regard to the forces have been formed. The results of this study indicate that the average resultant force primarily depends on the floor thickness to be deformed and the incremental depth in the tool path. This could be due to the variation in local stiffness of the sheet with change in floor thickness. The effect of tool diameter, deforming wall angle, and floor size is not significant.

Keywords. Deformation; thin section machining; single-point incremental forming (SPIF).

1. Introduction

Fabrication of complicated geometrical components and structures incurs large equipment and inventory costs. Reducing the manufacturing cost without compromising the quality of such components is a challenge. Smith *et al* [1] proposed a novel manufacture process—deformation machining (DM)—which is a combination of two processes, thin structure machining and single-point incremental forming (SPIF), as a solution. In this process, first, thin structures are machined from the bulk and then incrementally formed into the desired shape, resulting in the creation of lighter-weight components with novel and complex geometries. This process creates complex monolithic parts that were earlier assembled with simple tooling and equipment, therefore, enabling cost reduction in equipment, fabrication, and weight of the components. The potential application of such monolithic parts with complex geometries is in aerospace industry (e.g., mold lines of fuselage, avionic shelf, impellers, and pressurized bulk heads) [1], biomedical engineering (cranial plate, bone and joint support, prosthetics) [2], and heat transfer (irregular, curved fins). Studies on dimensional repeatability and fatigue life of DM components have shown that the DM components have shown better repeatability than SPIF components and better fatigue life than conventionally bent components [3].

First aspect of DM is the creation of thin structures out of the bulk raw material, which is done by thin structure machining. It is different from conventional machining due to the lack of stiffness of machined structure. Therefore, it requires different machining techniques such as use of long slender end mills [4] along with high-speed machining [5]. This process could be extensively used in aerospace and marine industries replacing assembled part with thin monolithic parts. Second aspect of DM is forming the machined thin structure into the desired shape. For this the SPIF technique is used. SPIF is a die-less forming process where a hemispherical single-point solid tool is used to deform the thin structure to a desired shape incrementally using computer numeric control [6]. In this process, the thin structure or sheet metal is deformed locally into plastic stage, enabling creation of complex shapes according to the tool path generated by a CNC machining center [7]. SPIF has enabled flexibility in creation of symmetric, asymmetric, and random shapes with sufficient amount of accuracy [8].

This process can be broadly classified into two, depending on the orientation of the deforming tool and the thin structure to be deformed: deformation machining stretching mode, where the deformation is along the axis of tool, resulting in stretching of the machined thin horizontal structure (thin floor) (figure 1a), and DM bending mode, where the deformation is perpendicular to the axis of the

*For correspondence

tool, resulting in the bending of thin vertical structure (thin wall) which was prior machined (figure 1b).

1.1 *Deformation machining stretching mode*

This paper presents a parametric experimental study on force measurements during deformation of the machined thin floor in DM stretching mode components. In this the deformation is along the axis of the tool, resulting in stretching of the thin horizontal structure. First, a thin horizontal section in a circular pocket is machined from the bulk material and then stretch formed into a frustum of cone. The applications of such a type of structure are in pressurized bulkheads and can also replace beaded panels to impart higher strength to the structures, which were earlier assembled to the flanges [1]. Measuring the magnitude of forces required in the process helps in optimum design of tools, fixtures, and machinery required for the process. Figure 2 depicts the schematic of thin structure machining and SPIF with the process parameters. Duflou *et al* [9] conducted the parametric experimental study on forces in SPIF. Aerens *et al* [10] predicted the forces both from experimentation and through finite element simulations. From the study of literature concerning the forces and formability in SPIF, it was observed that sheet thickness, vertical step size, and diameter of the forming tool are the major parameters influencing the forces in the incremental forming. In the present study, effect of process parameters, namely: (i) floor thickness (t), (ii) vertical step size of increment (Δz), (iii) forming tool diameter (d), (iv) deforming wall angle (α), (v) size of the thin machined structure (D), and (vi) shape of the deformed structure—conical and square pyramidal—on the forces has been recorded at different levels. Other process parameters that were deemed not so influential on the deforming forces, that is, feed, speed, and lubrication, were kept constant throughout the study.

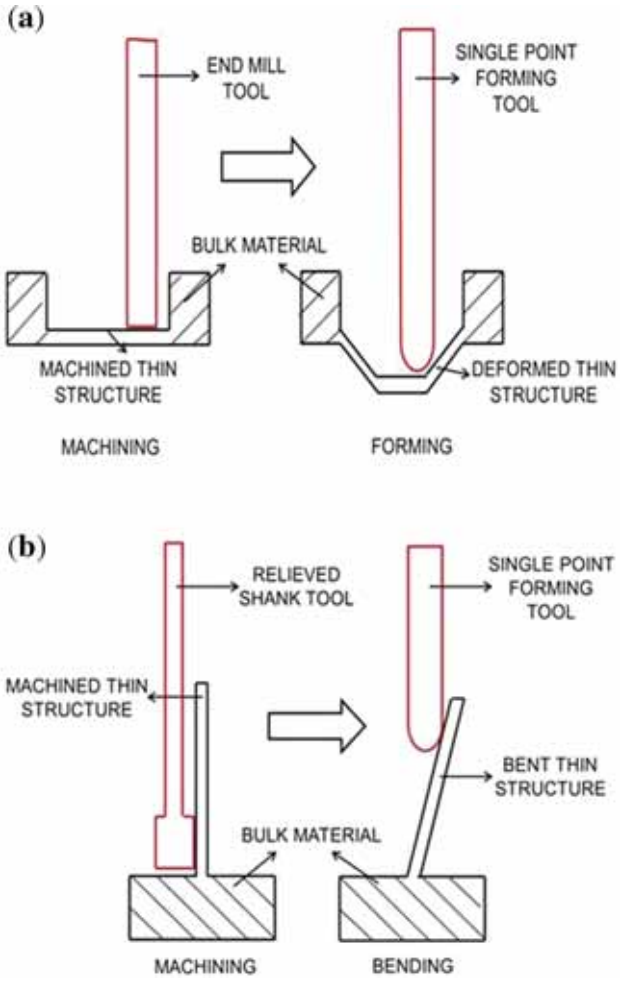

Figure 1. (**a**) Schematic of DM Stretching mode; (**b**) schematic of DM Bending mode.

2. Experimental methodology

Experiments have been carried out on a three-axis CNC vertical milling machine (Make: BFW, Model: VF 30 CNC VS). A fixture (figure 3a) has been designed and manufactured to carry out DM stretching mode operations. It consists of a holding plate and clamps for holding thick components, a backing plate for supporting the components during high-speed machining, and a base plate for providing overall stability of the fixture. During formation, the backing plate was removed from the fixture and the components were formed through a circular orifice in the holding plate. The exploded view of the fixture is shown in figure 3b. This fixture was clamped on Kistler 9257B six-component force dynamometer, a table-type force sensor, which was mounted on the CNC vertical milling machine table (figure 3c). The dynamometer was connected to Kistler 5070 8-channel charge amplifier. The amplifier amplifies the electrical signals generated during force exertion on the component by the tool and real-time data was recorded on a computer-based data acquisition system.

The material used in the present study is an aluminum alloy: AA 6063-T6, a commonly used alloy in aerospace, aviation, and marine industry. Table 1 depicts the mechanical properties of the alloy. The raw material was first machined to component size of 90 × 90 × 12 mm to be held in the fixture. Then, circular and square pockets of various sizes (D) were machined, creating thin floors of various thickness (t) employing high-speed plunge milling technique. Thereafter, the machined floor of desired thickness was incrementally formed into a conical and square pyramidal frustum using a single-point tool with hemispherical end. Contour tool path was employed for incremental forming. Table 2 shows various fixed parameters for machining and incremental forming. Variable parameters with levels are depicted in table 3.

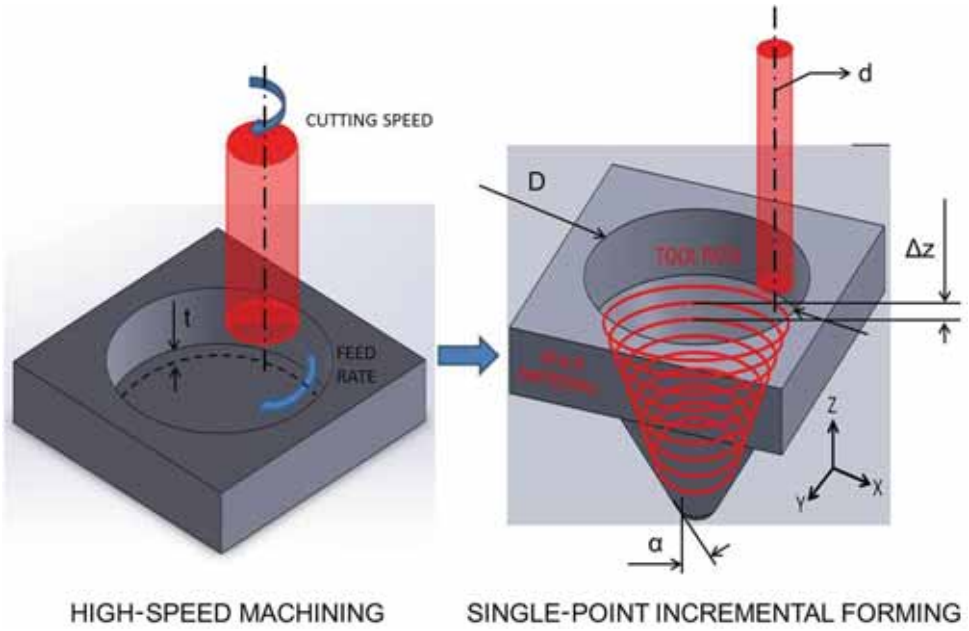

Figure 2. Schematic of thin structure machining followed by single-point incremental forming.

The forces were measured in three directions corresponding to Cartesian coordinate system, as shown in figure 2. After completion of one contour, the *Fz* component of the force first drops to minimum. When the tool plunges to the next contour, then reaches its peak value and finally stabilizes when the tool moves along the contour. *Fx* and *Fy* force components vary sinusoidal according to the tool position relative to the dynamometer axis in one contour. Axial component (*Fz*) of the force in thickness direction dominates as compared to horizontal components (*Fx* and *Fy*) in meridional and circumferential direction, respectively. In the current investigations, vector sum of the three force components *Fx*, *Fy*, and *Fz* is taken into account. The results are based on the average resultant vector sum of these forces after the *Fz* component stabilizes to a consistent value after the first few contours. This is primarily due to the bending effect of the thin floor initially in the first few contours prior to steady-state incremental forming. Figure 4a depicts all the three force components in incremental forming of frustum of cone with floor thickness 1 mm, incremental step size (depth) 0.5 mm, wall angle 45°, tool diameter of 10 mm, and thin floor size of 70 mm. Figure 4b shows the corresponding section of the component with all the dimensions.

3. Experimental design

In the current investigation, the experimentation has been divided into two parts: First, studying the effect of individual parameters on average resultant forces during DM stretching mode and developing a regression model for each of the process parameters. To achieve this, each parameter was varied sequentially and keeping the rest constant. The basic set of process parameters is given in table 4. The levels of each parameter are varied one by one keeping the other three basic sets of parameters constant. Secondly, studying the combined effect of all the parameters and developing a holistic regression model for average resultant deforming force and individual force components covering all the vital process parameters. For this four parameters with four levels each were considered, L_{16} orthogonal array was used. Signal-to-noise ratio was calculated using "Larger is better option" (Eq. 1) in all the cases:

$$\frac{S}{N} = -10 \log_{10}\left[\frac{\sum \frac{1}{y^2}}{n}\right] \quad (1)$$

where *y* denotes the average resultant forces, which is taken as the output response and *n* is the number of observations.

4. Experimental results

4.1 *Effect of individual parameters on the average resultant force*

4.1a *Influence of floor thickness* (*t*): The average resultant forces increase considerably with increase in floor thickness as seen in figure 5. The average resultant force rises up to 1120 N for a 2-mm floor thickness formed at 45° wall angle and 0.5 mm incremental depth, while for 0.8 mm floor thickness the force is limited to 330 N keeping other

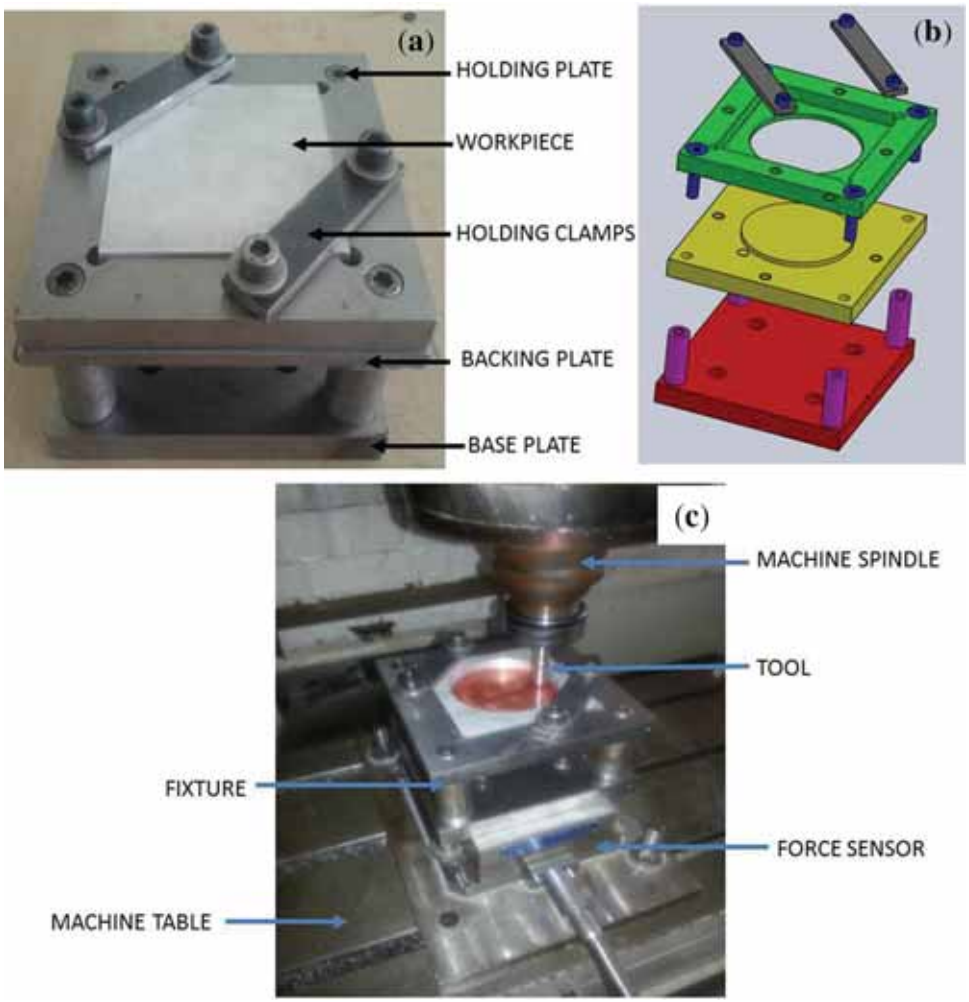

Figure 3. (**a**) Experimental fixture for DM stretching mode components; (**b**) exploded view; (**c**) fixture clamped on force sensor mounted on machine table.

Table 1. Properties of AA 6063-T6.

Properties	Density (gm/cc)	Melting point (°C)	Poisson's ratio	Modulus of elasticity (GPa)	Tensile strength (MPa)	Shear strength (MPa)	Proof stress
Magnitude	2.7	600	0.3	70	195	150	160 MPa at 0.2%

parameters constant. Therefore, it clearly implies that the floor thickness has a significant effect on the force values for DM stretching mode. Linear regressive model very well defines the trend for forces with varying floor thickness (Eq. 2).

$$F_{\text{avgr}} = 764.76\text{t} - 262.22. \quad (2)$$

4.1b *Influence of tool diameter* (*d*): Figure 6 shows the average resultant force values for different tool diameters used. It is evident that as the tool diameter increases, the magnitude of forces also increases, though marginally. Quadratic model fits in quiet well with the trends (Eq. 3). The reason for increase in forces as the tool size increases is the increase in contact zone (or plastic zone) between the tool and deforming thin floor.

$$F_{\text{avgr}} = -0.3529\text{d}^2 + 14.367\text{d} + 446.13. \quad (3)$$

4.1c *Influence of wall angle* (α): The average resultant force gradually increases with increase in wall steepness from 30° to 60° and then declines for 75° as visible from the trends in figure 7. The possible reason for such trends could be that the forces in *z* direction (*Fz*) are significant as compared to forces in *x* direction (*Fx*) and *y* direction (*Fy*). As the wall angle steepens the influence of *Fx* and *Fy*

Table 2. Fixed parameters for high-speed machining and SPIF.

Process parameters	High-speed machining	SPIF
Tool material	Tungsten carbide	Stainless steel 304
Tool diameter	16 mm	10 mm
Spindle speed	1200 rpm	100 rpm
Transverse feed (x, y)	500 mm/min	200 mm/min
Axial feed (z)	20 mm/min	10 mm/min
Depth of cut/incremental depth	1 mm	0.5 mm
Floor thickness	1 mm	N.A.
Deformed wall angle	N.A.	45°
Shape	Circular pocket	Conical
Size of pocket (thin floor)	70 mm	N.A.
Cooling/lubrication	Flood cooling	Mobil oil-40

Table 3. Variable parameters with levels.

Parameters	Levels
Deforming tool diameter	6, 8, 10, 12, 16 mm
Machined floor thickness	0.8, 1, 1.5, 2 mm
Incremental depth	0.25, 0.5, 0.75, 1 mm
Deforming wall angle	30, 45, 60, 75 mm
Size of pocket (thin floor)	Diameter 40, 50, 60, 70 mm
Deformed shape	Conical, square pyramidal

increases and therefore the average resultant value of force tends to decrease. The second possible reason for marginal decrease in the average resultant force could be attributed to the onset of failure. The drop in the force could be the result of localized necking as steep wall angle of 75° could be near the maximum achievable limits of the process. A quadratic regression equation fits well (Eq. 4) the trend of forces with increasing wall angle as shown in figure 7. The influence of the wall angle on the deforming forces is not as significant as that of floor thickness and incremental step size, but it probably gives an indication for the maximum achievable limits in terms of wall angle for the process.

$$F_{\mathrm{avgr}} = -0.0723\alpha^2 + 8.7993\alpha + 309.05 \qquad (4)$$

4.1d *Influence of step size* (Δz): Figure 8 shows the experimental results for average resultant force with varying incremental step size from 0.25 to 1.0 mm. It is clear that the magnitude of forces rises significantly. The average resultant force rises to 768 N for 1.0 mm incremental step size from 327 N for 0.25 mm step size, keeping other parameters constant. It can be seen that the average resultant force is directly proportional to the incremental step size and fits well with the linear trend (Eq. 5) shown in figure 8.

$$F_{\mathrm{avgr}} = 556.49\Delta z - 223.61 \qquad (5)$$

4.1e *Influence of thin floor size (D):* Influence of the size of thin floor is almost insignificant (with respect to the other parameters) on the average resultant forces, though marginal increase in the forces has been observed with reducing thin floor size (figure 9). This could be attributed to increased stiffness of lesser thin floor area circumcised by thick material. A linear regression curve fits in well with the force trends (Eq. 6).

$$F_{\mathrm{avgr}} = -17.508\mathrm{D} + 644.1. \qquad (6)$$

4.2 *Combined influence of process parameters*

From the experimental results of individual parameters on the average resultant force, thin floor size (D) was found out to be the least influential parameter. For combined influence and orthogonality of the experiment design, four process parameters—floor thickness (t), tool diameter (d), deforming wall angle (α), and incremental depth (Δz)—were considered. Values of average resultant force and individual force components for different experimental runs in Taguchi's L_{16} orthogonal array are given in table 5. Table 6 shows the results of ANOVA analysis for mean values carried out at 95% confidence level for average resultant force. Data presented in the table show that P values of floor thickness and incremental depth (highlighted) are less than or equal to 0.1, which endorses that these parameters have significant influence on the average resultant forces.

4.3 *Developing an empirical model for deforming force*

Analysis of variance (ANOVA) shows that floor thickness (parameter A) and incremental step depth (parameter D) have major influence on the average resultant force induced in incremental forming. A second-order polynomial equation used as expected function for regression analysis of average resultant force and individual average force components is given in the following equation.

$$\text{Average Force (N)} = C_1 + C_2\mathrm{A} + C_3\mathrm{B} + C_4\mathrm{C} + C_5\mathrm{D} + C_6\mathrm{A}^2 + C_7\mathrm{D}^2 + C_8\mathrm{AD} \qquad (7)$$

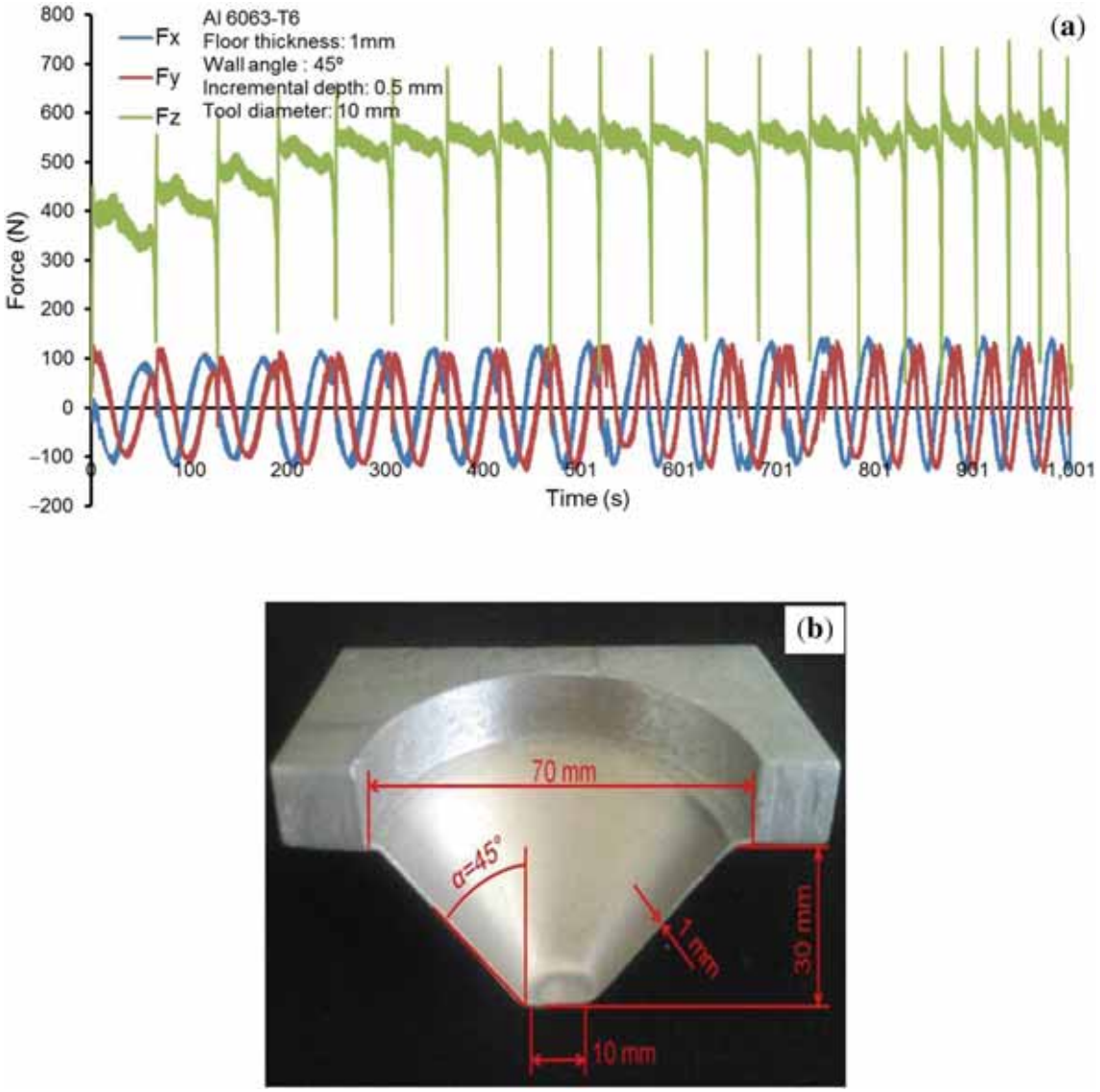

Figure 4. (**a**) Deforming force curves in three vector directions for conical profile; (**b**) Cross section of actual component with dimensional attributes.

Table 4. Parameters with basic levels.

Parameters	Floor thickness (t)	Tool diameter (d)	Incremental step size (Δz)	Wall angle (α)	Floor size (D)
Basic level	1 mm	10 mm	0.5 mm	45°	70 mm

where C_1 to C_8 are the constants. Square and interactive terms that include parameter B (tool diameter) and parameter C (wall angle) were intentionally removed from the equation as the parameters were insignificant according to the ANOVA analysis. The regression analysis was carried out at 95% confidence level with the Levenberg–Marquadt algorithm. The resultant empirical relations obtained from the analysis are given in Eqs. (8)–(10).

$$\text{Average Resultant Forming Force } \left(F_{\text{avg. resultant}}\right) \text{ (N)} = 300 - 147.3t + 14.0d - 9.6\alpha + 84.7\Delta z + 86.5t^2 - 9.9\Delta z^2 + 8.5t \cdot \Delta z \quad (8)$$

$$\text{Average axial force component } \left(F_{z\,avg.}\right) \text{ (N)} = 258.5 - 130.6t + 13.42d - 9.6\alpha + 79.1\Delta z + 79.1t^2 - 10.1\Delta z^2 + 8.48t \cdot \Delta z \quad (9)$$

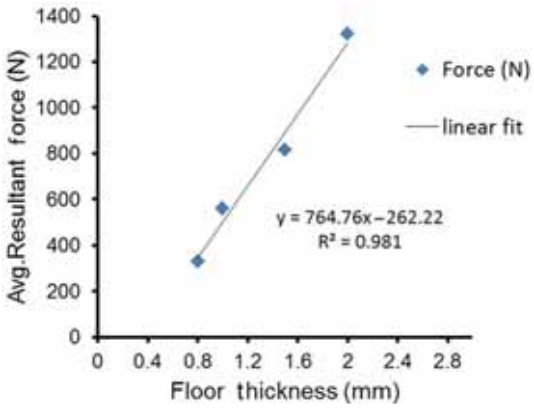

Figure 5. Graph of average resultant force vs. floor thickness.

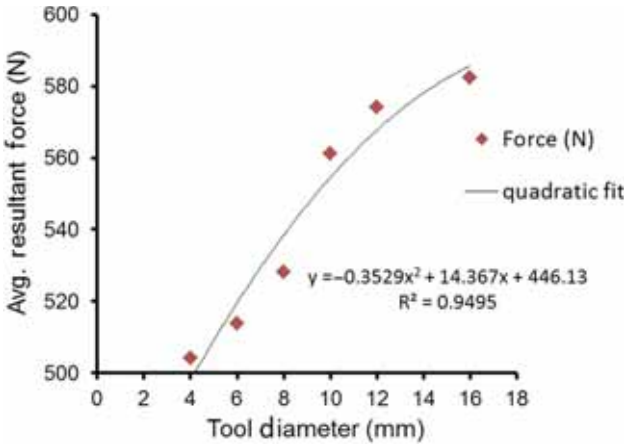

Figure 6. Graph of average resultant force vs. tool diameter.

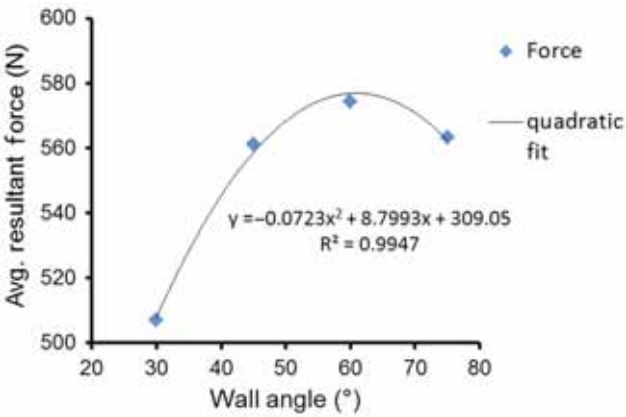

Figure 7. Graph of average resultant force vs. deforming wall angle.

$$\text{Average circumferential force component } \left(F_{x/y\ avg.}\right)\ (\text{N}) = 24.8 - 15.74\text{t} + 0.31\text{d} + 4.23\alpha + 10.62\Delta\text{z} + 11.11\text{t}^2 - 0.79\Delta\text{z}^2 + 0.06t \cdot \Delta\text{z} \quad (10)$$

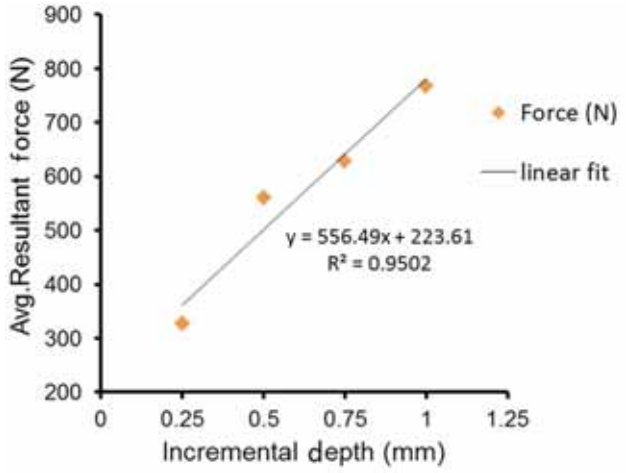

Figure 8. Graph of average resultant force vs. incremental depth.

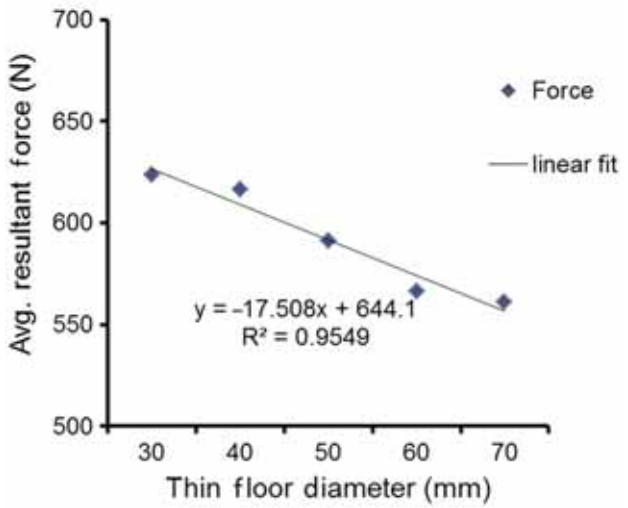

Figure 9. Graph of average resultant force vs. thin floor diameter.

4.4 *Experimental validation of the empirical model*

The empirical model presented in Eq. (7) has been compared and validated for different aluminum alloys at varied levels of parameters. The results are presented in table 7.

4.5 *Influence of shape of deformed structure*

Figure 10 depicts the forming force curves of the square pyramidal geometry with force components *Fx*, *Fy*, and *Fz*. The forces achieve a steady state after few contours same as in the conical geometry. For each contour, there are four peak forces corresponding to the tool movement at four corners of the shape. Influence of a square pyramidal

Table 5. Actual values of parameters in L_{16} orthogonal array along with forming force outputs.

Test run no.	(A) Floor thickness (mm)	(B) Tool diameter (mm)	(C) Wall angle (°)	(D) Incremental step depth (°)	Avg. resultant force (N)	Avg. force XY (N)	Avg. force Z (N)
1	0.8 (1)	6 (1)	30 (1)	0.25 (1)	320.45	34.62	285.32
2	0.8 (1)	8 (2)	45 (2)	0.5 (2)	382.41	45.66	337.65
3	0.8 (1)	10 (3)	60 (3)	0.75 (3)	413.25	56.67	363.68
4	0.8 (1)	12 (4)	75 (4)	1.0 (4)	470.59	66.12	411.81
5	1.0 (2)	6 (1)	45 (2)	0.75 (3)	610.48	73.28	542.98
6	1.0 (2)	8 (2)	30 (1)	1.0 (4)	657.79	81.43	590.99
7	1.0 (2)	10 (3)	75 (4)	0.25 (1)	461.85	65.98	411.86
8	1.0 (2)	12 (4)	60 (3)	0.5 (2)	580.43	78.38	523.66
9	1.5 (3)	6 (1)	60 (3)	1.0 (4)	850.10	116.40	770.82
10	1.5 (3)	8 (2)	75 (4)	0.75 (3)	823.76	114.98	753.87
11	1.5 (3)	10 (3)	30 (1)	0.5 (2)	798.18	91.66	733.62
12	1.5 (3)	12 (4)	45 (2)	0.25 (1)	780.38	98.35	716.44
13	2.0 (4)	6 (1)	75 (4)	0.5 (2)	1321.10	183.57	1213.23
14	2.0 (4)	8 (2)	60 (3)	0.25 (1)	1177.55	159.93	1076.50
15	2.0 (4)	10 (3)	45 (2)	1.0 (4)	1456.79	180.19	1332.35
16	2.0 (4)	12 (4)	30 (1)	0.75 (3)	1404.94	171.46	1289.22

Table 6. ANOVA for means (average resultant forces).

Source	DF	Seq SS	Adj SS	Adj MS	F	P
Floor thickness	3	2,006,648	2,006,648	668,883	685.83	**0.000**
Tool diameter	3	4561	4561	1520	1.56	0.362
Deforming angle	3	7091	7091	2364	2.42	0.243
Incremental depth	3	67,481	67,481	22,383	22.95	**0.014**
Residual error	3	2926	2926	975		
Total	15	2,088,273				

Table 7. Validation experiment results and comparison.

	Parameters						
Material	Floor thickness (mm)	Tool diameter (mm)	Deforming angle (°)	Incremental depth (mm)	Experimental force result (N)	Empirical value (N)	Percentage difference
Al 6063-T6	1.0	6	30	1.0	643.28	627.52	2.5% increase
	2.0	8	45	0.5	1297.78	1260.26	2.9% increase
Al 6101-T6	0.8	10	75	0.25	267.24	288.65	7.4% decrease
	1.5	12	60	0.75	894.12	953.29	6.2% decrease
Al 99.5% pure	1.0	6	30	1.0	554.75	627.52	11.4% decrease
	2.0	8	45	0.5	1123.73	1260.26	10.8% decrease
Al 3003	0.8	10	75	0.25	265.37	288.65	8% decrease
	1.5	12	60	0.75	887.26	953.29	6.9% decrease

geometry in comparison with the conical frustum on the deforming forces has been experimentally performed. From the ANOVA analysis of the process parameters, floor thickness was the most influential parameter on the deforming forces. Therefore, the experimental comparison was performed on varying floor thickness and by keeping the rest of the parameters same (refer table 4). An increase in the average resultant forces for the square pyramidal shape in comparison with the conical shape at varying floor thickness has been observed (figure 11). This could be attributed to the rise of force value at the corners in pyramidal shape.

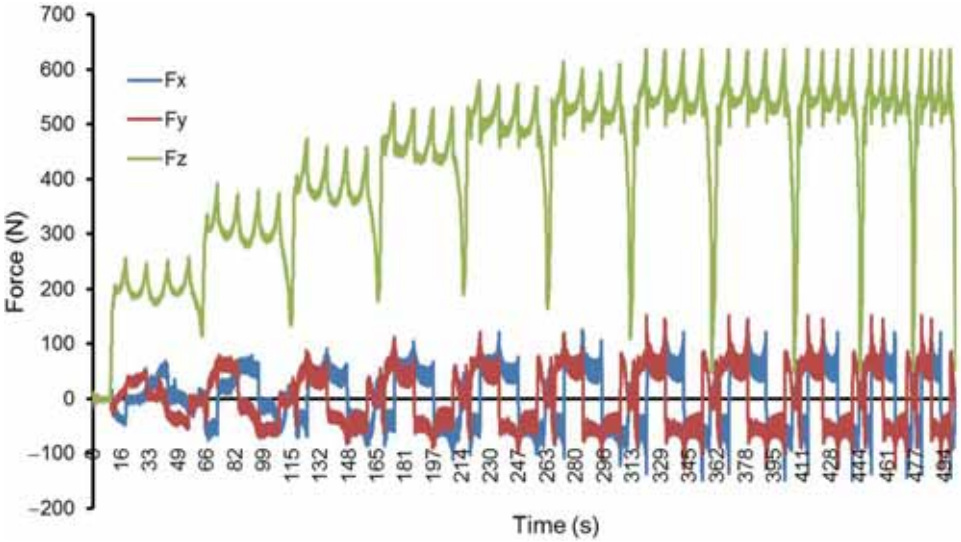

Figure 10. Deforming force curves in three vector directions for square pyramidal profile.

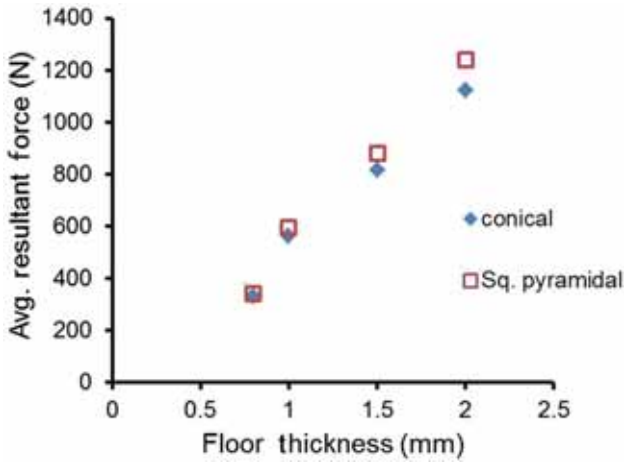

Figure 11. Comparison of average resultant force for conical and square pyramidal profile at varying floor thickness.

4.6 *Comparison of deforming forces in DM stretching mode with incremental sheet metal forming*

Deformation machining components have been produced from the bulk extruded billets machined to thin floor structures and then incrementally formed into the desired shape. Whereas, in incremental sheet metal forming, thin rolled sheets were formed incrementally into desired shape. Tensile tests were conducted on machined extruded billet, extruded billet, and rolled sheet as per ASTM E8 with gage length of 10 mm in three directions of lay: parallel, perpendicular, and diagonal (45°), considering anisotropy associated with the direction of lay. Then, average nominal stress was calculated as

$$\sigma_{\text{avg}} = \left(\sigma_{\text{perp}} + 2\sigma_{\text{diag}} + \sigma_{\text{parl}}\right)/4 \tag{11}$$

where σ_{perp} is stress perpendicular to lay, σ_{parl} is stress parallel to lay, and σ_{diag} is stress diagonal (45°) to lay [11].

From the tensile test graph (figure 12) a noticeable increase in the average nominal stress can be seen for extruded billet in comparison with the rolled sheet of AA 6063-T6. Tensile strength of the machined billet improves marginally in comparison to the extruded one primarily due to the work hardening associated with it.

Comparison of deforming forces in DM stretching mode with incremental sheet metal forming has been performed at varying floor/sheet thickness. From figure 13 it is evident that the average resultant forces in DM stretching mode are significantly larger than the incremental sheet metal forming. This endorses that the prior machining and extrusion processes in DM have a significant bearing on the deforming forces in comparison to the rolled sheets.

5. Summary and conclusion

The results of this study indicate that average resultant force during DM process primarily depends on floor thickness to be deformed and incremental depth in the tool path. Among these two, the floor thickness is observed to be the most significant parameter. Whereas the effect of tool diameter, deforming wall angle, and floor size were found not as significant. Empirical relation between the average resultant force and individual force components for investigated parameters was established using regression analysis with good level of accuracy. The model has been compared and validated for different aluminum alloys at varied levels of parameters, within an error range from 2.5

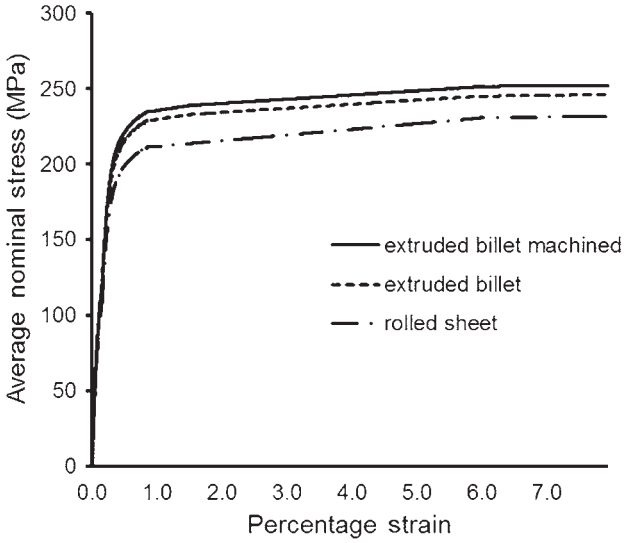

Figure 12. Tensile test graph of the raw samples.

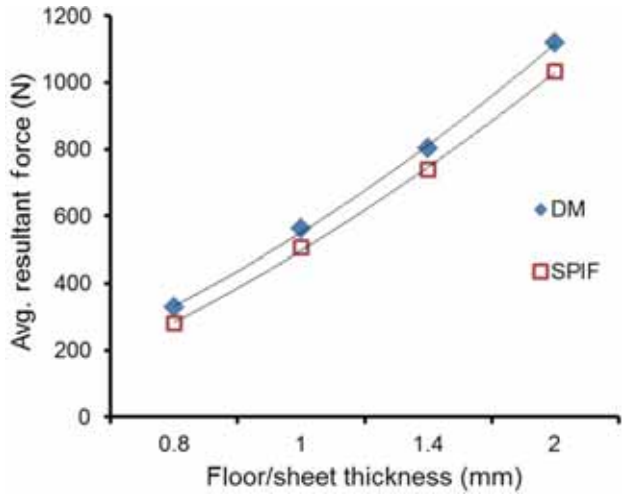

Figure 13. Comparison of average resultant forces of deformation machining with SPIF.

to 11.4%. The influence of shape of the formed component on the average resultant forces has also been studied and found to be dependent on the geometry (figure 11). Forces during DM process and SPIF on sheet metal have been carried out and were observed to be more during DM process. It could be due to the work hardening of the component during machining, prior to deformation.

Acknowledgements

The authors acknowledge DST Project SB/FTP/ETA-254/2012 for providing the financial support and IIT Ropar for providing the basic facilities.

References

[1] Smith S, Woody B, Ziegert J and Huang Y 2007 Deformation machining—a new hybrid process. *CIRP Ann. Manuf. Technol.* 56(1): 281–284

[2] Ambrogio G, De Napoli L, Filice L, Gagliardi F and Muzzupappa M 2005 Application of incremental forming process for high customized medical product manufacturing. *J. Mater. Process. Technol.* 162: 156–162

[3] Agrawal A, Smith S, Woody B and Cao J 2012 Study of dimensional repeatability and fatigue life for deformation machining bending mode. *Trans. ASME: J. Manuf. Sci. Eng.* 134(6): 061009

[4] Tlusty J, Smith S and Winfough W 1996 Techniques for the use of long slender end mills in high-speed milling. *Ann. CIRP* 45(1): 393–396

[5] Smith S and Dvorak D 1998 Tool path strategies for high speed milling aluminum work pieces with thin webs. *Mechatron. J.* 8(3): 291–300

[6] Echrif S B M and Hrairi M 2011 Research and progress in incremental sheet forming processes. *Mater. Manuf. Process.* 26(11): 1404–1414

[7] Malhotra R, Reddy N V and Cao J 2010 Automatic 3D spiral tool path generation for single point incremental forming. *J. Manuf. Sci. Eng.* 132(6): 061003

[8] Hussain G, Al-Ghamdi K A, Khalatbari H, Iqbal A and Hashemipour M 2014 Forming parameters and forming defects in incremental forming process: Part B. *Mater. Manuf. Process.* 29(4): 54–460

[9] Duflou J R, Tunckol Y, Szekeres A and Vanherck P 2007 Experimental study on force measurements for single point incremental forming. *J. Mater. Process. Technol.* 189: 65–72

[10] Aerens R, Eyckens P, Van Bael A and Duflou J R 2010 Force prediction for single point incremental forming deduced from experimental and FEM observations. *Int. J. Adv. Manuf. Technol.* 46: 969–982